Large Deformation Mechano-Optical and Dynamical Phase Behavior in Uniaxially Stretched Poly(ethylene naphthalate)

C. I. Martins and M. Cakmak*

Polymer Engineering Institute, University of Akron, Akron, Ohio 44325-0301

Received December 3, 2004; Revised Manuscript Received February 28, 2005

ABSTRACT: Uniaxial deformation behavior of PEN films in the rubbery state is investigated as a function of processing temperature, draw rate, and molecular weight (M_w). Real-time measurement of true stress−true strain and birefringence of the films during the process of stretching is obtained by using a novel instrumented uniaxial stretching machine that couples the spectral birefringence system with the real-time strain detection system. This enables quantitative measurement of true stress−true strain and birefringence, enabling quick and nonstop measurement of stress−optical behavior (SOB) of PEN. A three-regime SOB was obtained for PEN films: (i) regime I—stress optical rule applies with a stress optical constant (SOC) of 27.5 GPa^{-1}; following this regime the behavior become nonlinear in (ii) regime II and birefringence rises steeply; finally in (iii) regime III, birefringence reaches a plateau while stress increases. All regimes are affected by the temperature, rate, and M_w. Decreasing temperature and increasing stretching rate and M_w extend the range of regime I over which the material remains amorphous. Regime II and III slopes were found to be dependent on rate and M_w. Measurement of strain rate indicates that affine deformation holds until the end of regime I, rising sharply in regime II, as a result of spontaneous deformation. The strain rate rapidly decreases to zero when regime III starts. The peak in strain rate coincides with the fast increase of birefringence during regime II. According to WAXD and DSC studies, the material remains amorphous in the regime I. Right after the transition to the regime II, the amorphous chains are extremely oriented but possess low translational order, which prevents them from crystallizing. Further stretching the structure evolves very rapidly to a crystalline structure, with approximately 40% crystallinity that is maintained throughout the regime III at the end of which finite chain extensibility prevents further changes in the structure. A model representing the structural mechanisms followed from the amorphous to the crystalline state is suggested. Both rate and temperature have a significant effect on the structural development of PEN: at intermediate to high rates and low temperatures a semicrystalline structure is obtained whereas at very high temperatures and low rates the structure remains completely amorphous despite the large deformation that has been applied. On the basis of the these data, a dynamic phase diagram was constructed.

Introduction

Uniaxial deformation of amorphous PEN films in the rubbery state within T_g + 30 °C is accompanied by necking that occurs as result of a cooperative realignment of the naphthalene groups parallel to each other and to the surface of the film, resembling an isotropic to nematic structural transition.[1] This behavior is not common in other materials, especially in its close homologue PET. Elimination of neck can be achieved by stretching at very low rates or fairly high temperatures[2] or by blending with other polymers such as PEI,[3] PEI/PEEK,[4] and PC.[5] Blending showed the complete elimination of necking; however, it also hindered the crystallization behavior of PEN. Recently an increased attention is given to PEN/PET blends[6−8] with the objective of increasing barrier and thermal properties of PET.

Studies on structural details including stress−optical behavior during deformation in rubbery state of PEN are rather limited: Ito et al.[9] investigated the effect of drawing temperature and drawing rate on the stress−birefringence relationship of PEN in uniaxial and simultaneous equal-biaxial mode. Additional studies were reported on stretching of PEN films,[1,2,10−12] fiber spinning,[13−16] injection molding,[17,18] and welding[19] with primary focus on the processing effect on the development of structure in relation to physical properties including mechanical performance, optical properties, and the texture developed. These "after the fact" studies did not lend themselves in unravelling complex sequence of "structural events" as later processes tend to mask earlier ones. For example, the existence of a mesophase structure as an intermediate state in the crystallization process of polymers as suggested by Flory[20] and Keller[21] is easily masked by subsequent crystallization if the materials are examined after all the physical processes are completed. Mesophase seems to appear in PEN,[22−24] PET,[25−27] and PET/PEN copolymers[28,29] as a precursor of strain-induced crystallization, however for a very short period of time (≈0.2 s as observed for PET[25]) and at very specific conditions, such as the combination of low temperatures (close to T_g) and fast rates. Very recently, Kawakami et al.[30] proposed a mechanism for the structural development during drawing of PET above T_g. Three steps composed the mechanism: first there is the formation of a mesophase state that provides the nucleation sites for crystallization and then imperfect crystals are formed which start the formation of a network and simultaneously cause strain hardening. Crystal growth, crystal perfection, and crystal orientation follow as the strain increases. Finally, the process proceeds with a stable crystal growth. These observations were based on the synchrotron WAXD technique and load−strain curves.

Although the synchrotron technique allows the detection of crystalline structure beyond about 5−10% crys-

* To whom all correspondence should be addressed. E-mail: cakmak@uakron.edu.

10.1021/ma047499s CCC: $30.25
Published on Web 04/16/2005

tallinity levels, it is not sensitive to most of the local structural organization processes prior to crystallization that take place in the amorphous rubbery state. Birefringence as an overall measure of the optical anisotropy of materials is a robust quantitative technique that gives insights as to the mechanistic changes in these early stages of structural organization processes particularly when it is coupled with true stress and strain measurements.[31−33] In this regard, in this paper, an investigation on the mechano-optical behavior of PEN films in the rubbery state as influenced by temperature, rate, and molecular weight is presented. The main objective is to elucidate the connections between various stages of the mechano-optical behavior of PEN and the associated structural mechanisms. The mechano-optical studies were performed with the real-time mechano-optical measurement system, and these are augmented with additional off-line additional structural measurement techniques.[34,35]

Experimental Procedure

Materials. Two commercial grades of PEN films with intrinsic viscosity (IV) of 0.54 and 0.67 dL/g and 0.75 mm average thickness were used in this study. Both films were kindly provided by M&G Polymers Co. For convenience, the former is designated by LPEN (low molecular weight PEN) and the last by HPEN (high molecular weight PEN).

On-Line Birefringence and True Mechanical Behavior Measurements. A uniaxial stretching machine developed in our group was used to simultaneously determine the mechanical and optical properties of PEN films during deformation. The machine is essentially composed of three parts: the uniaxial stretching machine with environmental chamber, the spectral birefringence system, and a laser-based width measurement system. Real-time measurements of optical retardation, sample width at the stationary midsymmetry plane, and force are recorded simultaneously. This mid-symmetry plane location was made possible by designing the sample shape to be the narrowest in this region and having two crossheads that move in opposite directions, unlike standard uniaxial testers where one crosshead moves. In this system, the laser micrometer continuously monitors the width of the sample at the mid-symmetry plane by precision measurement of the sample shadow generated by a very narrow laser light sheet(∼0.2 mm). This allows continuous determination of cross-sectional area even under the conditions when necking start to occur at this mid-symmetry plane. Assuming (1) simple uniaxial extension and (2) incompressibility, time variation of the local thickness is calculated, and thus birefringence, local true stress, and local true strain are determined using

$$\text{true strain} = L_t/L_0 - 1 = (W_0/W_t)^2 - 1$$

$$\text{true stress} = F_t/(W_t D_t) = F_t/[(W_t^2/W_0)D_0]$$

where W_0 and D_0 are initial width and thicknesses and F_t,W_t, and D_t are time variation of force, width, and thicknesses. D_t is calculated using uniaxial symmetry $D_t = (W_t/W_0)D_0$. True strain rate was calculated from true strain vs time curves.

As will be shown in this paper, the samples typically start at 0% crystallinity and reach ultimate crystallinity of about 40% at the final stretched state. The volume change between these states is approximately 5% ($\rho_c = 1.407$ g/cm^3,[36] $\rho_a = 1.325$ g/cm^3 [37]). Since the width of the sample is continuously monitored during deformation and crystallinity development is concentrated toward the end of stretching, the error committed by the incompressibility assumption is acceptable. In addition, assuming all of the dimensions are equally affected by this volume change and we are already measuring one of the three dimensions continuously, this measurement reduces the committed error. We have also verified this assumption with off-line thickness and width measurements in comparison with the real-time thickness values calculated from width measurements. These data are shown in Figure 1 where correlation is quite linear at all deformation levels.

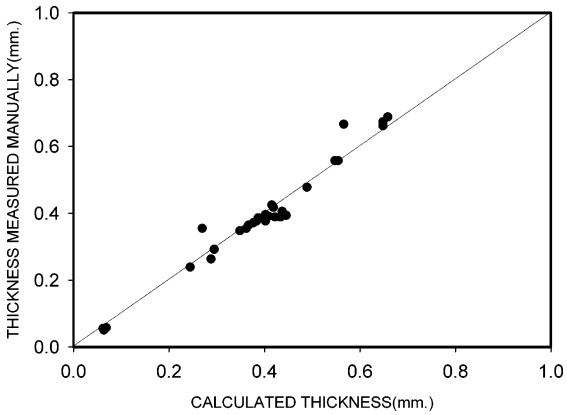

Figure 1. On-line (using uniaxial assumption) vs off-line thickness measurements (using precision micrometer).

Table 1. Stretching Conditions

	stretching conditions
temperature	130, 135, 140, 145, 150, 155, 160 (°C)
rate	2, 10, 20, 100, 200 (mm/min)
	0.001, 0.005, 0.01, 0.05, 0.1 (s^{-1})
stretch ratio	maximum 5×

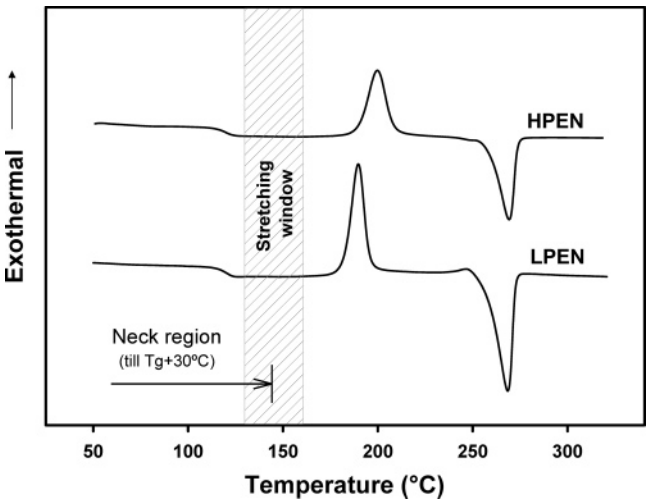

Figure 2. DSC thermograms of as-received PEN films. The films exhibit necking behavior up to about 140 °C.

Additional details of the spectral birefringence, true stress, and true strain measurement system can be found elsewhere.[34,35,38,39] In the spectral birefringence technique both crossed and parallel polarized light intensity were collected in the visible range using fiber-optic spectrometers, and retardation at the wavelength of 546 nm was extracted as described in detail elsewhere.[34,35,38,39]

Sample Preparation and Experimental Conditions. Dumbbell-shaped specimens were cut from the original melt cast and amorphous films with the following dimensions: 75 mm long, 40 mm wide, and 30 mm wide in the narrowest region. The samples were clamped and fixed in the arms of the uniaxial stretching system inside the environmental oven. The distance between clamps was taken as 30 mm. Prior to each experiment, the sample was thermally equilibrated in the oven for 10 min. After stretching at the desired conditions, the samples were cooled by room temperature air before they were removed from the clamps.

The conditions used in this study are indicated in Table 1. For reference the range of temperature applied is indicated in the DSC thermogram of Figure 2.

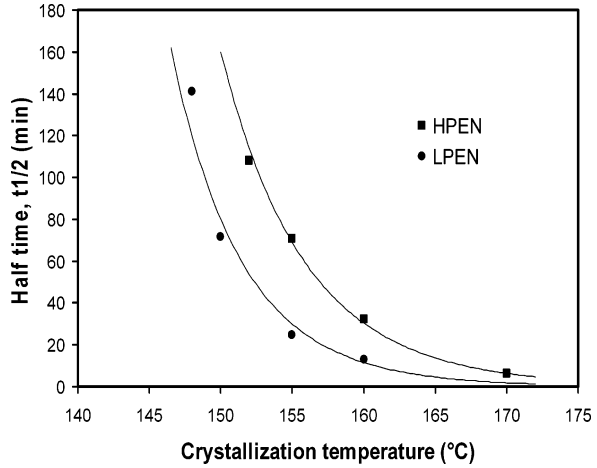

Figure 3. Half-time crystallization of HPEN and LPEN.

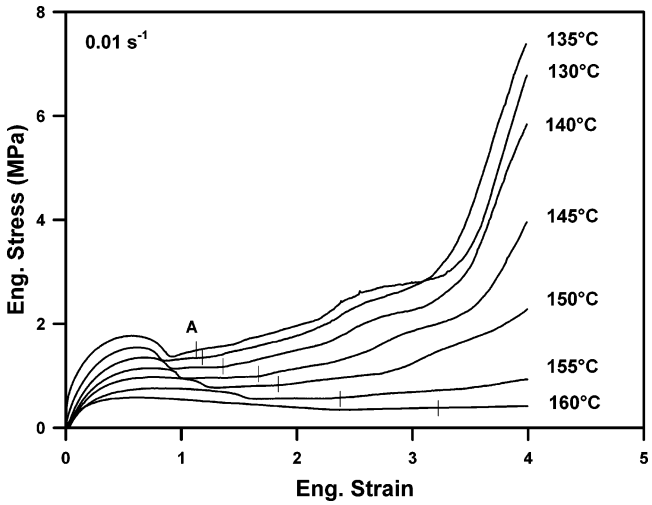

Figure 4. Temperature effect on the engineering stress−engineering strain curve of HPEN stretched at 0.01 s^{-1} (20 mm/min).

Thermal Characterization. Thermal properties of PEN films were measured using a universal 2920 MDSC V2.6A TA Instruments DSC. The samples of approximately 6−10 mg were scanned at heating rate of 10 °C/min in a dry nitrogen atmosphere. The reported transition temperatures (T_{cc}, T_m) are referring to the peak maximum position. The degree of crystallinity was determined using ΔH_c enthalpy of melting and enthalpy of crystallization estimated by the DSC curves and the heat of fusion of 100% crystalline (ΔH_f^0) to be 103.4 J/g.[40]

Isothermal crystallization of PEN was investigated by rapidly heating the amorphous cast PEN films to the following temperatures—148, 150, 155, and 160 °C in the case of LPEN and 152, 155, 160, and 170 °C in the case of HPEN—and keeping the sample isothermal for a predefined time.

X-ray Measurement. A Bruker AXS generator equipped with a copper target tube and two-dimensional detector was used to obtain the one-quadrant WAXD patterns of uniaxially oriented samples. The generator was operated at 40 kV and 40 mA with a beam monochromized to Cu Kα radiation. A typical detector-to-sample distance of 11.5 was used. An exposure time of 10 min was applied.

Results and Discussion

Thermal Properties of PEN. As-received melt cast samples are essentially amorphous (~5% crystallinity) as shown in DSC thermograms of both films (Figure 2). They exhibit T_g at 120 °C and T_m at 270 °C. Crystallization from amorphous state during heating occurs earlier in LPEN having relatively shorter and more mobile chains as compared to HPEN; consequently, the peak position of cold crystallization (T_{cc}) of LPEN is observed at 190 °C and HPEN at 200 °C.

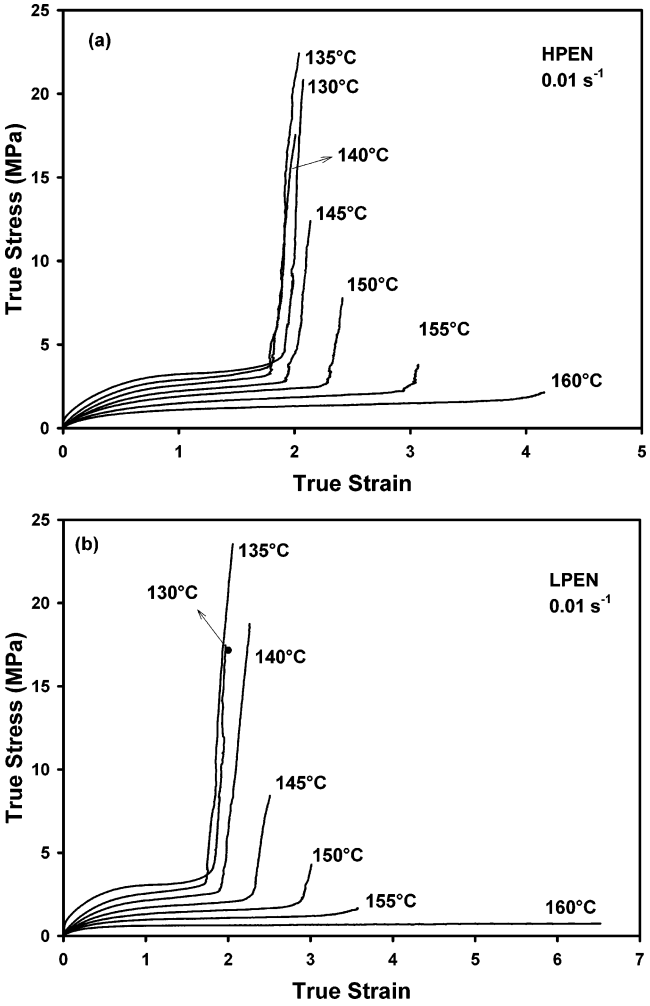

Figure 5. Temperature effect on the true stress−true strain curve of (a) HPEN and (b) LPEN stretched at 0.01 s^{-1} and stretch ratio of 5×.

Isothermal Crystallization of PEN. Although isothermal crystallization of PEN has been investigated by several authors,[41−43] the aim here is to assess the time required to induce thermal crystallization at temperatures up to 170 °C, where the typical stretching experiments were made. These analyses allow the selection of the thermal equilibration and deformation times shorter than the time for the onset of crystallization and thus avoid complications arising from thermally induced crystallization.

In Figure 3, the half-time crystallization, $t_{1/2}$, of LPEN and HPEN is plotted as a function of crystallization temperature taken between 145 and 170 °C. As would be expected, $t_{1/2}$ decreases with the increase of temperature and increases with the increase of M_w for a given temperature. This in turn indicates that the crystallization rate increases as the cold crystallization temperature is approached. At 170 °C, for example, the $t_{1/2}$ is only 2 min for LPEN and 6 min for HPEN, which is a quite short time for this temperature to be applied in studies of strain inducing crystallization. These results are close to those reported by our group earlier.[42] At 160 °C the $t_{1/2}$ increased to 13 min for LPEN and 32 min for HPEN. The rate of thermal crystallization has

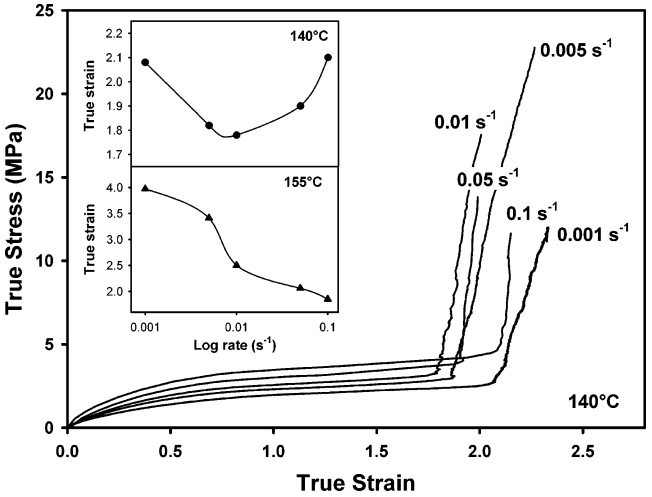

Figure 6. Rate effect on the true stress−true strain curve of HPEN stretched at 140 °C and stretch ratio of 5×. (Inset: critical true strains at the onset of strain hardening for 140 and 155 °C are shown as a function of nominal strain rate.)

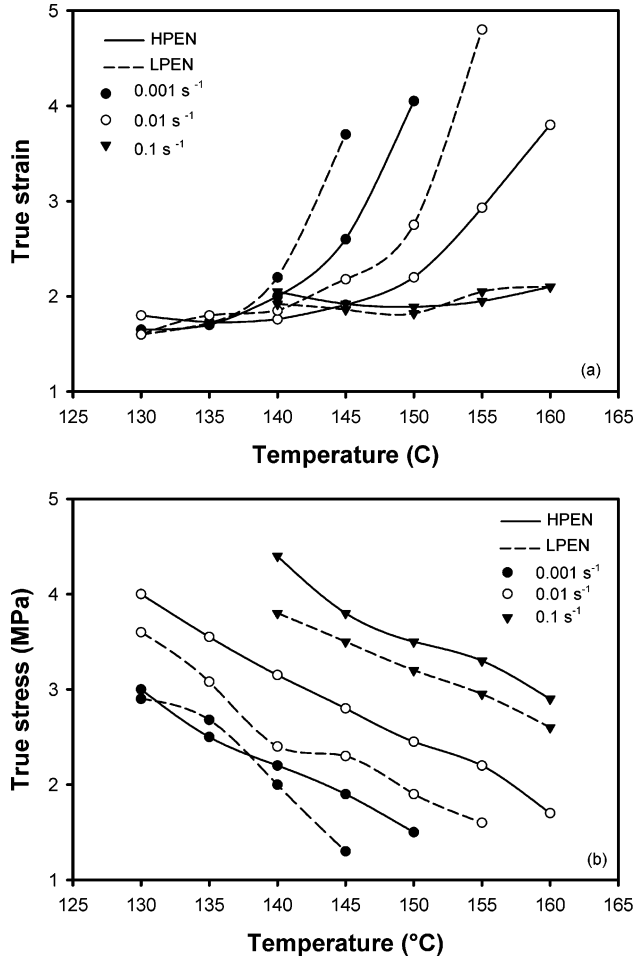

Figure 7. True strain and true stress values at onset of strain hardening as a function of temperature, rate, and M_w.

decreased considerably so it is safe to consider this temperature in the stretching experiments as well consider an equilibration time period of approximately 10 min without being concerned with thermal crystallization prior to the beginning of the stretching process. Another concern is that half-time crystallization can be reached within the total time of the experiment, i.e., equilibration time plus stretching time, especially when

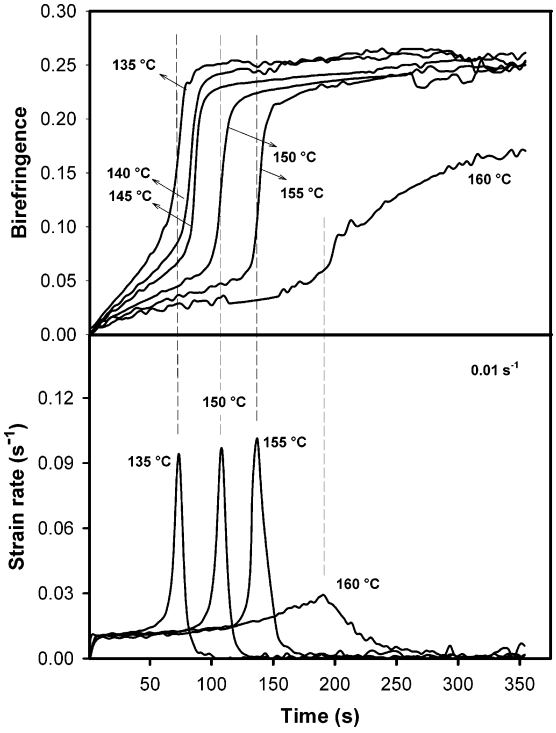

Figure 8. Change of birefringence with time (top) and change of strain rate with time (bottom) for HPEN stretched at several temperatures and rate of 0.01 s^{-1}.

low rates (0.001 s^{-1}) together with high stretch ratios are applied. For example, a sample stretched at 0.001 s^{-1} for a total stretch ratio of 5× has the following times: equilibration time of 10 min and stretching time of 60 min. Thus, a total of 70 min is needed. This means that above 150 °C for LPEN and 155 °C for HPEN thermal crystallization can occur during the stretching process. Additional discussion regarding this subject will be provided in future sections.

Mechanical Behavior. PEN deforms uniformly up to a critical structural state beyond which it exhibits neck formation as evidenced in Figure 4. This is a characteristic behavior of PEN films as observed by Cakmak et al.[1] and results from the cooperative realignment of the naphthalene groups parallel to each other and to the surface of the film, resembling a disorder−nematic order (in direction normal to the surface) like transition. This behavior can persist to temperatures as high as 20−30 °C above its T_g. The use of higher processing temperatures and/or lower stretching rates suppresses this mechanism.[1,2] The results plotted in the figure shows that the neck formation is reduced with the increase of temperature, as observed by the decrease of yielding stress and the broadening of the region between yielding point (initial maximum) to the following minimum drawing stress; however, necking is not entirely eliminated even for high temperatures. Considerable strain hardening is observed for temperatures below 150 °C, yet at higher temperatures the material exhibits "taffy-pull (chewing gum)" characteristics.

The true mechanical behavior of HPEN and LPEN shown in Figure 5 does not indicate stress drop when neck occurs as the true stress is calculated on the basis of the actual cross-sectional area of the sample that is continuously changing during stretching. The main advantage of true stress−strain data is that it clearly identifies the onset of strain hardening in the material.

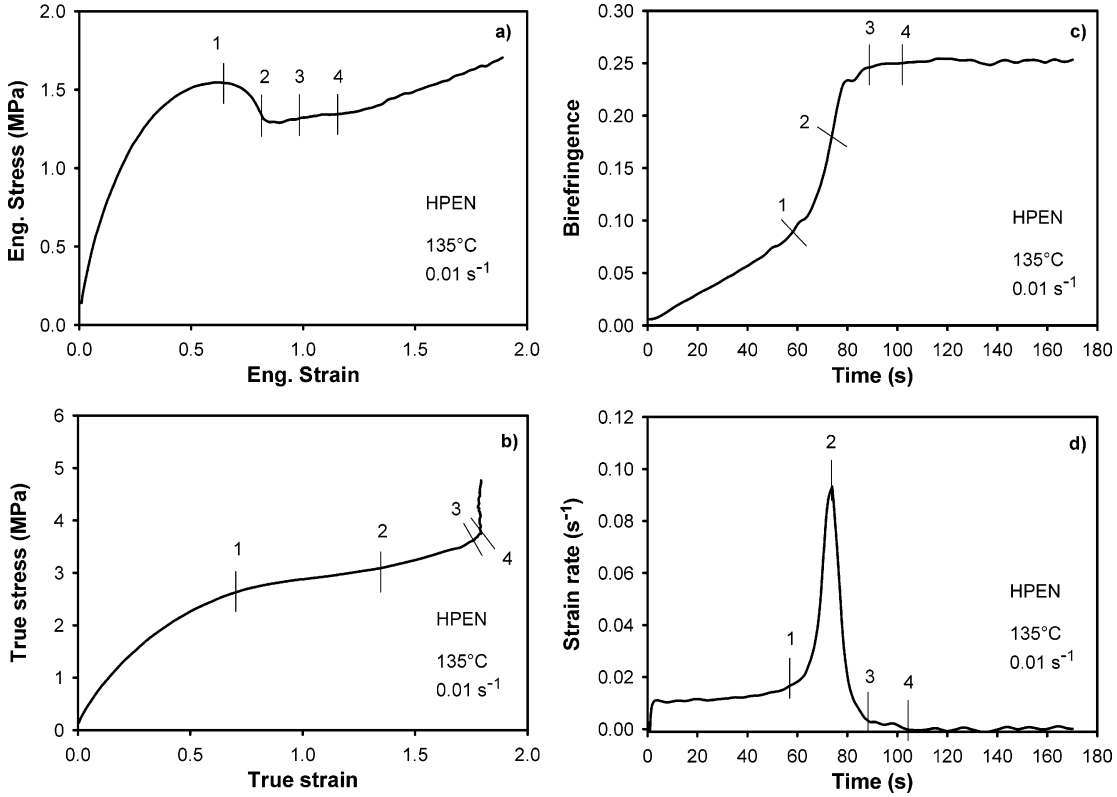

Figure 9. Comparison of data for HPEN deformed at 135 °C and 0.01 s^{-1}: (a) engineering stress−engineering strain curve, (b) true stress−true strain curve, (c) birefringence vs time, and (d) strain rate vs time.

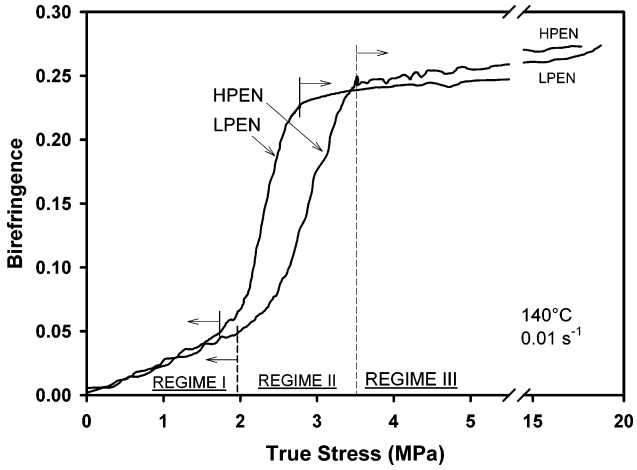

Figure 10. Molecular weight effect on the mechano-optical behavior of PEN stretched at 140 °C and 0.01 s^{-1} and stretch ratio of 5×.

This appears as a very sharp rise in the stress at a specific true strain depending. Once strain hardening occurs, further increase in strain becomes minimal.

For comparison, a letter A and a small vertical line marks in the engineering stress−strain curve (Figure 4) the onset of strain hardening point identified in true stress−strain (Figure 5a) curves. Although a good correlation between the locations of strain hardening point taken in the two types of plots is observed when using the technique of tracing a tangent from −1 in x axis to the curve, the strain at strain hardening is not the same in both cases. Engineering strain predicts the onset of strain hardening to occur at lower strains.

The increase of processing temperature shifts the strain at the onset of strain hardening to higher true strains, and this strain hardening eventually disappears altogether when deformation takes "taffy-pull" character at 160 °C. LPEN and HPEN exhibit similar behavior although taffy-pull behavior appears at lower temperatures in the case of LPEN, reflecting the decrease in the entanglement density in the material. In addition, for the same stretching conditions, LPEN shows lower draw stresses as compared to HPEN.

The influence of stretching rate on the onset of strain hardening is complex, as is shown in Figure 6. The behavior deviates from the expected steady decrease of strain at the onset of strain hardening. This value first decreases and after showing a minimum begins to increase with further increase of stretching rate (see inset at 140 °C). On the other hand, at higher temperatures (155 °C) the expected decrease of strain at the onset of strain hardening is observed.

A possible interpretation for the behavior observed at 140 °C is as follows: at high rates the molecules are forced to orient rapidly in the stretching direction, and thus chain relaxation or chain slippage is restricted, preventing the initiation of the crystallization process. Consequently, a delay of strain hardening is observed. This tendency agrees with the observations of Blundel[44] which indicated that when materials are stretched very fast, crystallization takes place after deformation has been completed.

Figure 7 summarizes the effect of temperature, rate, and M_w on the onset of strain hardening of PEN. This dependency is given in terms of the true strain and true stress values corresponding to the onset of strain hardening for each condition. As shown in Figure 7a, a critical true strain value between 1.75 and 2.10 is needed for strain hardening of the material. This range is relatively insensitive to temperature and M_w when

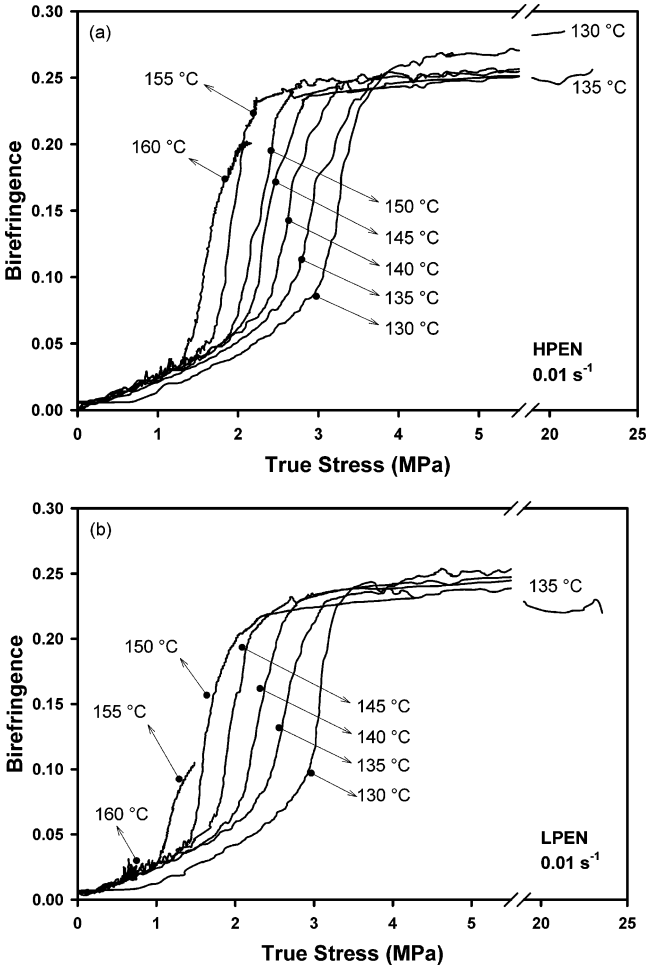

Figure 11. Temperature effect on the mechano-optical behavior of (a) HPEN and (b) LPEN, stretched at rate of 0.01 s^{-1} to a final draw ratio of 5×.

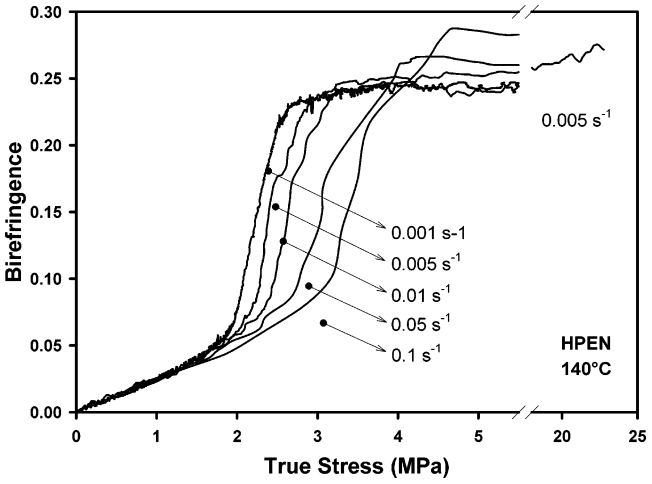

Figure 12. Rate effect on the mechano-optical behavior of HPEN stretched at 140 °C to a final draw ratio of 5×.

the highest rate is applied or when the material is stretched below 140 °C. For other rates (0.001 and 0.01 s^{-1}), an exponential deviation from the above trend is observed. In this case higher strains are needed as the temperature increases, rate decreases, and M_w decreases.

The stress at the onset of strain hardening decreases linearly with the increase of temperature and decrease

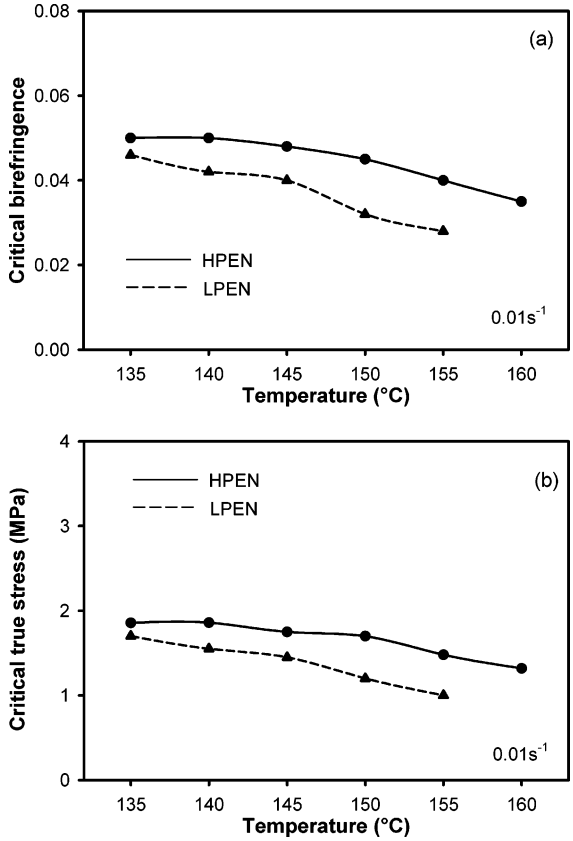

Figure 13. Critical values of true stress and birefringence at the point of deviation from linearity of the stress optical rule—M_w and temperature effect.

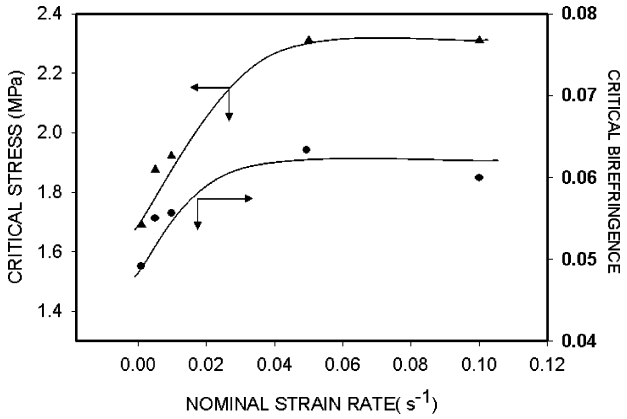

Figure 14. Critical values of true stress and birefringence at the point of deviation from linearity of the stress optical rule—rate effect.

of the rate and molecular weight, as expected (Figure 7b)

Optical Behavior. The birefringence change during deformation follows three stages (Figure 8 top): first the birefringence increases slowly, then a sharp rise of birefringence at almost constant time is observed, and finally the birefringence reaches a saturation level that corresponds to the plateau observed in this figure.

The orientation levels reached at each stage are greatly dependent on the stretching temperature; specifically, the higher the temperature, the lower is the level of birefringence achieved and the larger is the delay in the transition between each stage. In addition, at 160 °C, the stage II is substantially suppressed.

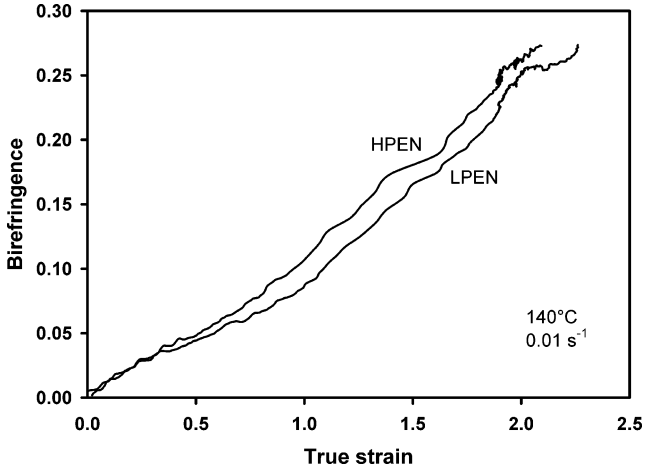

Figure 15. Molecular weight effect on the strain−optical behavior of PEN stretched at 140 °C, 0.01 s^{-1}, and stretch ratio of 5×.

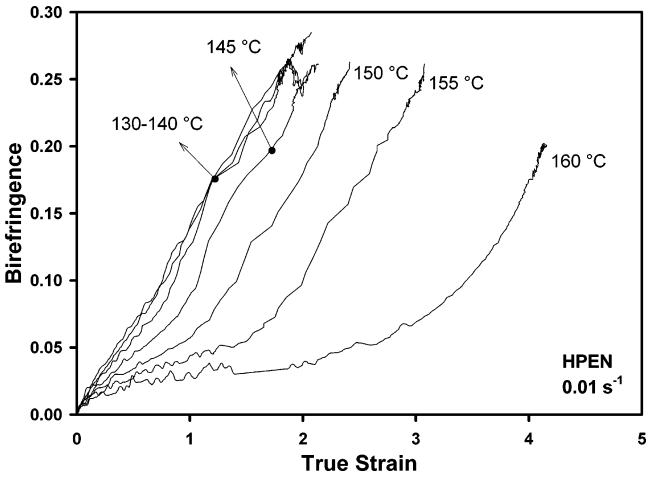

Figure 16. Temperature effect on the strain−optical behavior of HPEN stretched at rate of 0.01 s^{-1} to a final draw ratio of 5×.

With the exception of 160 °C, the final birefringence level attained ranges from 0.24 to 0.26 that are quite high. PEN exhibits high intrinsic birefringence (maximum theoretical value). Inoue et al.[45] and Miyata et al.[46] reported values of 0.33 and 0.344 (for α crystal structure), respectively. Huijts and Peters[47] reported a value of 0.487 for PEN and Kim and Cakmak[13] a value around 0.791 for crystalline phase and 0.75 for amorphous phase, based on high-speed melt spinning studies where the intrinsic birefringence was estimated by extrapolation of actual data.

Strain Rate Behavior. The true strain rate extracted from true stress−strain behavior is shown in Figure 8 (bottom) for 0.01 s^{-1}. The results indicate that at constant crosshead separation speed the strain rate at the midsection of the sample is not constant. At early stages of deformation, the strain rate is around 0.01 s^{-1} for all temperatures, following affine deformation behavior as it corresponds to the macroscopic stretching rate applied by the stretching machine. Then, strain rate sharply rises, signifying spontaneous deformation at the very local level in which this measurement is made. Following this, strain rate rapidly decreases ultimately reaching zero value at the midsection of the sample before the macro deformation is completed. The peak position is also strongly dependent on the temperature and thus moves to longer times as the temperature increases while the initial affine deformation stage becomes longer. An abrupt change in the behavior of the material occurs between 155and 160 °C for which the peak broadens considerably and the maximum strain rate is very low compared to the other cases. The origin of this behavior seems to be related to the taffy pull characteristics of PEN at this temperature, stemming from sluggish crystallization character combined with low stress generation due to decreased interchain friction at this temperature range (see Figure 5).

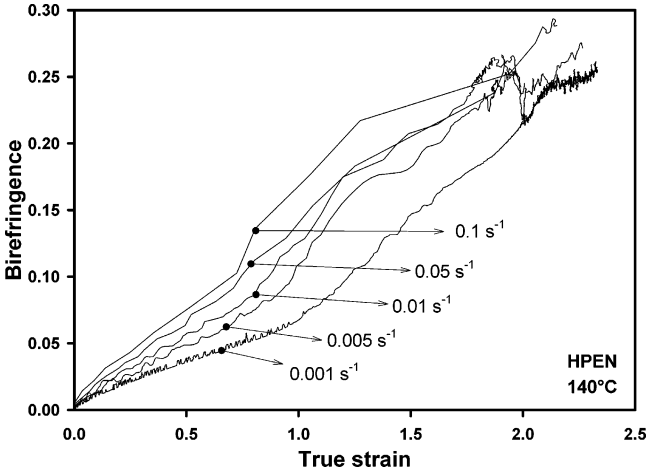

Figure 17. Rate effect on the strain−optical behavior of HPEN stretched at 140 °C to a final draw ratio of 5×.

The strain rate results are directly correlated to the birefringence changes observed in the material. In the affine deformation stage (Figure 8), birefringence increases linearly with time. When the strain rate accelerates, so does the birefringence. At a certain time, the strain rate reaches a maximum and starts decreasing again, while the birefringence is still increasing sharply. Finally, the birefringence reaches a constant value when the strain rate becomes zero. A possible explanation for these results is that after a certain level of chain elongation a process of spontaneous deformation begins that induces the fast increase of chain orientation of the material, causing the rise of both birefringence and strain rate. Eventually the strain rate reaches a maximum and starts decreasing thereafter. Still, this rate is much higher than the one initially set, and thus the birefringence keeps increasing sharply. When the molecules attain their finite extensibility, chain orientation stops (birefringence plateau), and consequently no more straining is allowed, resulting in zero strain rate.

There have been arguments on the "coil-to-stretch" (or coil-to-deformed coil) transition as the mechanism causing the sudden increase of birefringence of polymers under elongational flows. At critical strain rate, the chains pass from a deformed random coil to a near fully extended state.[48,49] For PEN, although coil-to-stretch mechanism is clearly observed, it is augmented by the existence of necking in the rubbery state, as is shown in Figure 9. The numbers marked in the figure make the correspondence between the critical transitions observed in the strain rate and birefringence (Figure 8) with the transitions in the mechanical behavior of HPEN (Figures 4 and 5), stretched at 135 °C and 0.01 s^{-1}.

It is observed that affine deformation is followed during the early stages of deformation of the material. As soon as yielding starts (beginning of plastic deforma-

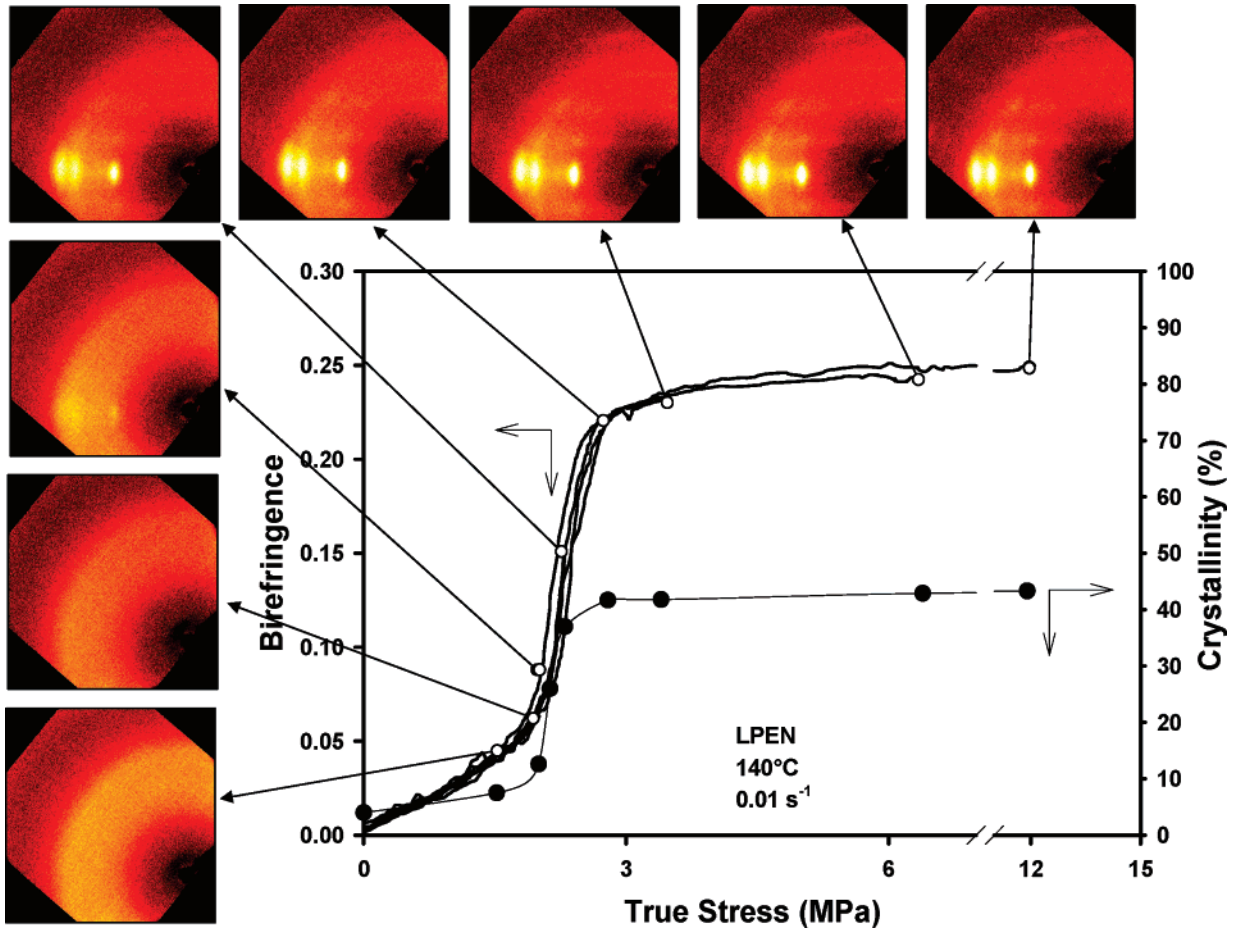

Figure 18. Mechano-optical behavior of LPEN at different stretch ratios with correspondent WAXD patterns and % of crystallinity.

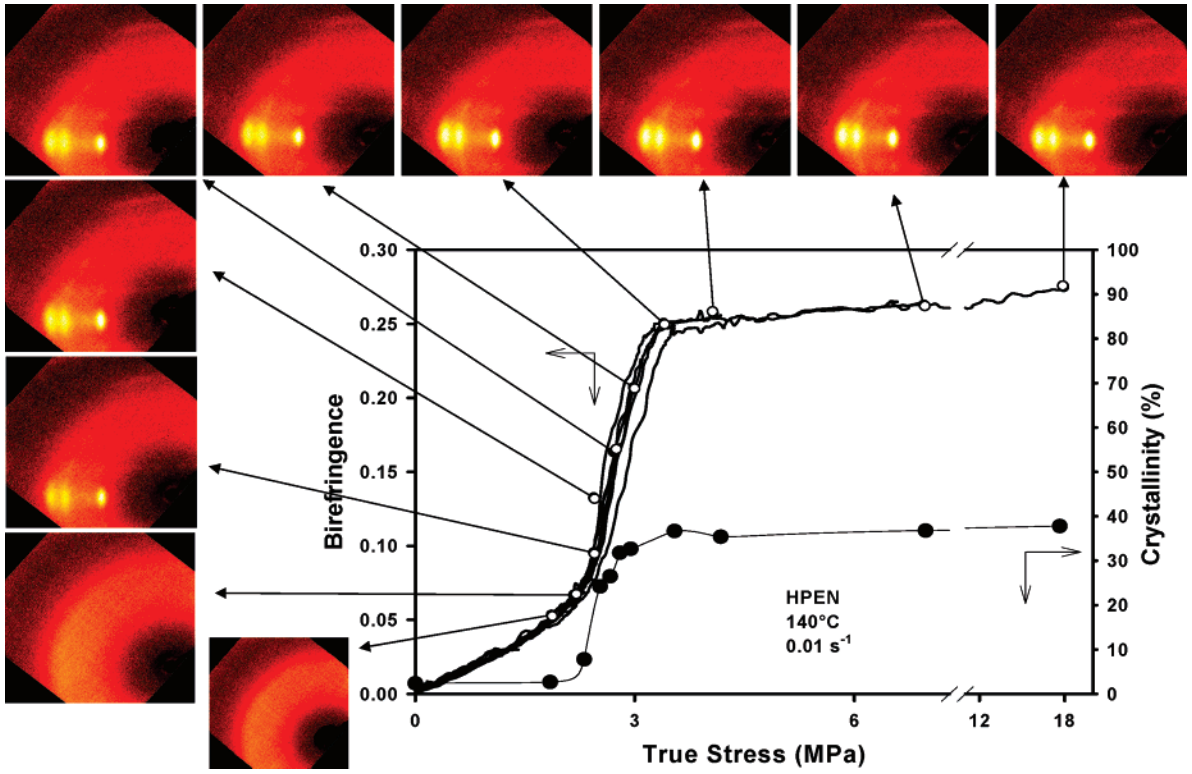

Figure 19. Mechano-optical behavior of HPEN at different stretch ratios with correspondent WAXD patterns and % of crystallinity.

tion indicated by point 1 of Figure 9a), the strain rate increases sharply to its maximum (point 2 of Figure 9d), indicating that the increase of strain rate is associated with necking of PEN in the rubbery state, which in turn results in the fast alignment of the molecules in the machine direction (point 1 to 2 in Figure 9c). When the

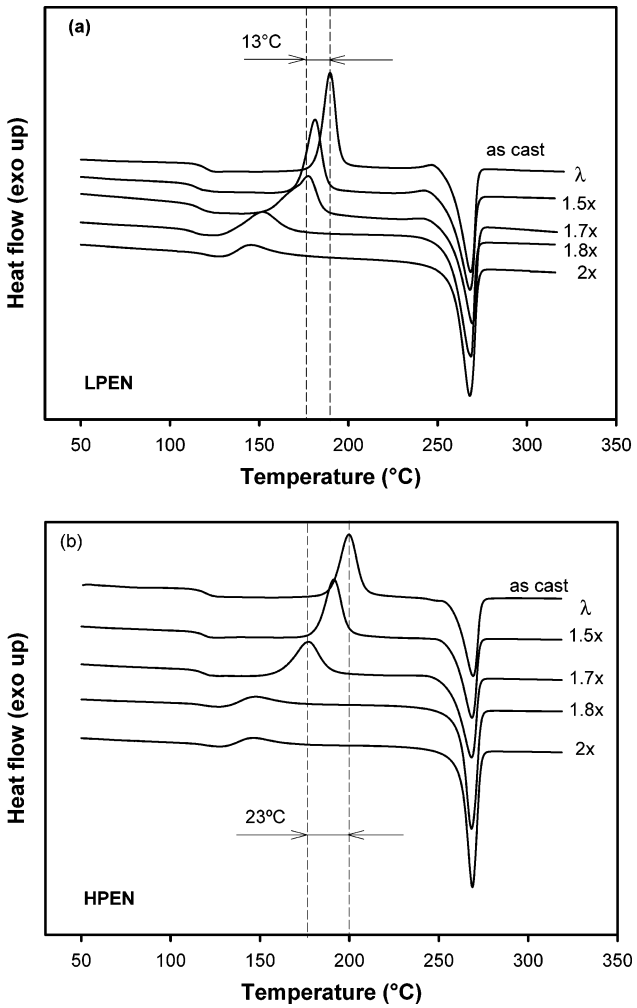

Figure 20. DSC thermograms of (a) LPEN and (b) HPEN samples stretched at 140 °C and 0.01 s^{-1} at different stretch ratios.

molecules start to resist once again to the applied deformation (point 2 of Figure 9a), the strain rate starts to decrease until it reaches an almost zero value (point 3 of Figure 9d). At this point, the birefringence continues to increase. Soon after, the strain hardening of the material occurs (point 4), and thus the strain rate reaches its zero level and no more change in birefringence is observed. This process occurs in a very short period of time (around 40 s) and for true strains below 1.2.

Mechano-Optical Behavior (MOB). Three distinct stress−optical regimes are observed for PEN, as shown in Figures 10−12: (i) regime I, where the birefringence increases linearly with stresses, i.e., stress optical rule applies with a stress optical constant (SOC) of 27.5 GPa^{-1}; (ii) regime II, where fast increase of birefringence is observed at almost a constant stress, and (iii) regime III, where stress increases while birefringence gradually reaches a plateau.

M_w, temperature, and rate affect the regimes of MOB; however, SOC is independent of all of them (except at low temperatures such as 130 °C, as it will be discussed shortly). Regime I is extended to higher stress and birefringence levels as the molecular weight increases, temperature decreases, and rate increases. This is shown quantitatively in Figures 13 and 14 with critical birefringence and critical stress representing deviation points from regime I. The birefringence plateau of regime III seems to be independent of temperature (excluding 130 °C for HPEN) but rate and M_w dependent; i.e, higher birefringence levels are achieved as the rate and M_w increase, indicating the importance of entanglement density in these developments. A final level of birefringence between 0.23 and 0.28, depending on the stretching condition applied and M_w used, was obtained.

At 130 °C the stress optical behavior exhibits a different trend: a fast increase in the stress is observed with little change in the birefringence and then recovers and follows the stress optical behavior as for the other temperatures. This behavior is attributed to the typical glassy contribution of polymers, observed near the glass transition temperature, as also was observed by others.[50]

At high temperatures (above 155 °C for LPEN and 160 °C for HPEN), neither of the materials reaches regime III of the stress−optical behavior, as depicted in Figure 11. Moreover, LPEN stretched at 160 °C, remaining entirely in regime I. This behavior corresponds to the conditions at which the material behaved like taffy-pull (Figure 5).

It is clear that a temperature decrease and/or a rate increase extend the linear stress−optical regime (regime I). This observation is in agreement with the results obtained by Ito et al.[9] Their results however do not show the existence of three regimes of the stress optical behavior as found in this research. The stress optical constant determined by Ito et al. was 13 GPa^{-1}. Other authors, such as Iizuka et al.,[51] Inoue et al.,[52] and Okamoto et al.,[53] reported the following values: 16.1, 12.4, and 18 GPa^{-1}, respectively. These results also differ from the result obtained in this investigation.

Strain Optical Behavior. The effect of molecular weight, temperature, and rate on the strain optical behavior of PEN is represented in Figure 15, Figure 16, and Figure 17, respectively. Clearly, the general strain optical behavior is nonlinear. However as will be noted below, it exhibits noteworthy temperature-dependent behavior.

As the M_w decreases, temperature increases, and rate decreases, the efficiency to orient the polymer chains decreases with strain as the relaxation process increasingly becomes significant with the above-mentioned changes.

The effect of temperature on the strain-optical behavior of HPEN is very significant. For example, at temperatures between 130 and 140 °C, a linear dependency between birefringence and true strain with a strain optical constant of 0.1376 is observed. This behavior points that a higher efficiency of deformation in the absence of relaxation effects occurs at temperature up to 140 °C even though the material is supposedly in the rubbery state. This unusual behavior changes between 140 and 145 °C where the birefringence increases with the decrease of true strain. At higher temperatures, the birefringence increases continuously with the increase of strain; however at low strains, the rate of change of birefringence is lower as compared to high strains. At high enough temperatures, i.e., above 155 °C, the birefringence increases very slowly while the material is being strained, forming a plateau, after which the birefringence starts increasing considerably. The fast increase of birefringence in this region approaches the rate of birefringence change encounter at temperatures between 130 and 140 °C.

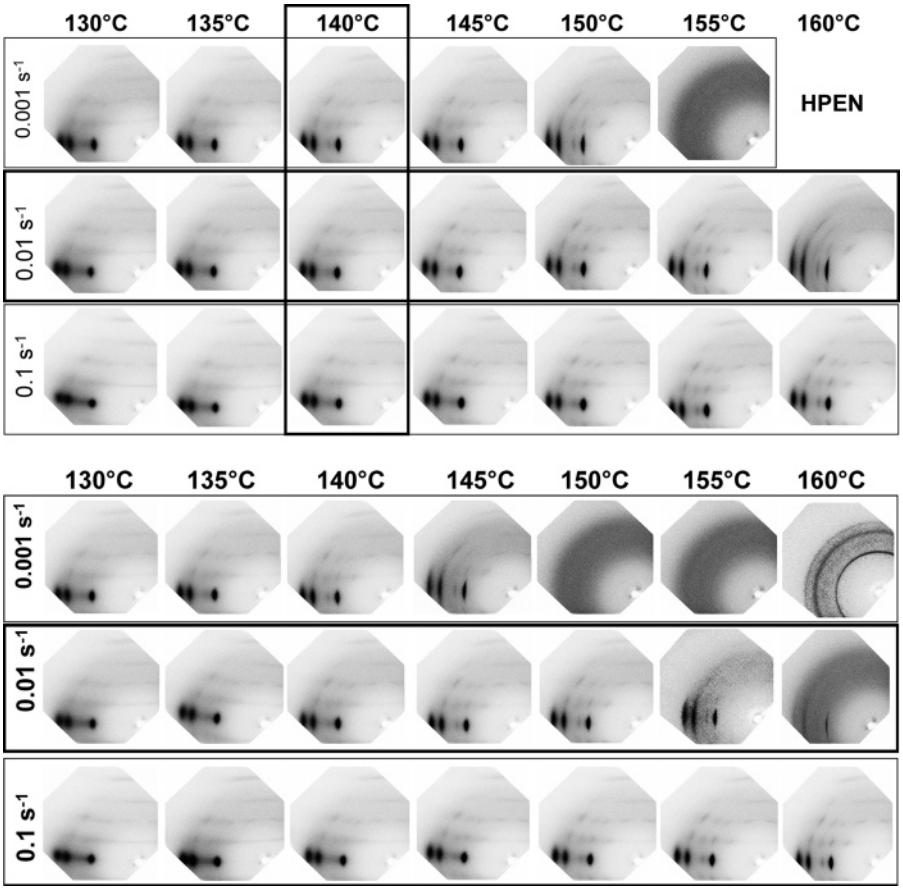

Figure 21. WAXD patterns of HPEN (upper) and LPEN (lower) at temperatures ranging from 130 to 160 °C and at rates 0.001, 0.01, and 0.1 s^{-1}. All the samples were stretched to a stretch ratio of 5×.

The rate of deformation affects also the strain optical behavior of the material, revealing the appearance of a two-regime behavior as the rate decreases, in the same way as it occurred for intermediate temperatures.

Structural Studies. A. Effect of Deformation. To clarify the molecular mechanisms responsible for the transitions observed in the mechano-optical behavior of PEN, a series of samples were stretched to different stretch ratios at the temperature of 140 °C and rate of 0.01 s^{-1}, and X-ray and DSC were taken afterward.

In Figure 18 the mechano-optical behavior of LPEN is shown together with the WAXD patterns and crystallinity level determined by DSC. In regime I, where SOR applies, the material remains amorphous as indicated by the broad halo in the WAXD pattern and the very low level of crystallinity attained. In the transition from regime I to II, although the WAXD pattern shows a completely amorphous structure, the percentage of crystallinity slightly increases to around 8%. A significant increase is observed thereafter, reaching a value above 20% when the first signs of crystalline peaks appear in the WAXD pattern. This occurs at birefringence levels of ≈0.1. The WAXD pattern is characterized by very sharp equatorial peaks, indicating a small fraction of the structure exhibiting near perfect orientation along the stretching direction lacking translational order in the same direction as evidenced by the absence of off-equatorial crystalline peaks. The structure evolves with the sharpening of the equatorial peaks corresponding to α-form[54] (010), (100), and ($\bar{1}$10) planes. As the deformation proceeds in regime III, diffused off-equatorial peaks increasingly become better defined, signifying the establishment of three-dimensional order in the oriented crystalline domains. During deformation in regime II, a substantial increase in crystallinity (around 43%) is observed. This property levels off in regime III. No significant structural change seems to be occurring in this regime, unless the emergence of ($\bar{2}$20) crystalline reflection belonging to crystal. This peak have been reported to appear in films,[1] however, only when stretched at 165 °C.

Figure 19 shows the structural changes occurring in HPEN. In this case, the amorphous structure observed in regime I is transformed into very highly oriented ordered regions still containing translational disorder at the start of the regime II. The equatorial diffraction peaks appear at a birefringence level of 0.1, similarly to LPEN. The appearance of the latter peaks also accompanies a rapid rise in crystallinity to 25% at the end of this regime. This structure evolves with the perfection of the crystalline phase during the remainder of regime II and regime III (appearance of well-defined off-equatorial peaks). A final crystallinity level of 40% is attained for HPEN, which is slightly lower than LPEN.

It is shown by Figure 18 and Figure 19 that the structural evolution mechanism observed in the transition to regime II is M_w dependent. For the same orientation level (birefringence of 0.1), HPEN shows a more developed crystalline structure as compared to LPEN. This is directly attributed to differences in entanglement density in these materials. Having a higher entanglement density in HPEN leads to a higher density long range "telegraphing" connectivity between the chains as the number of entanglement junctions per chain increases with an increase in the molecular

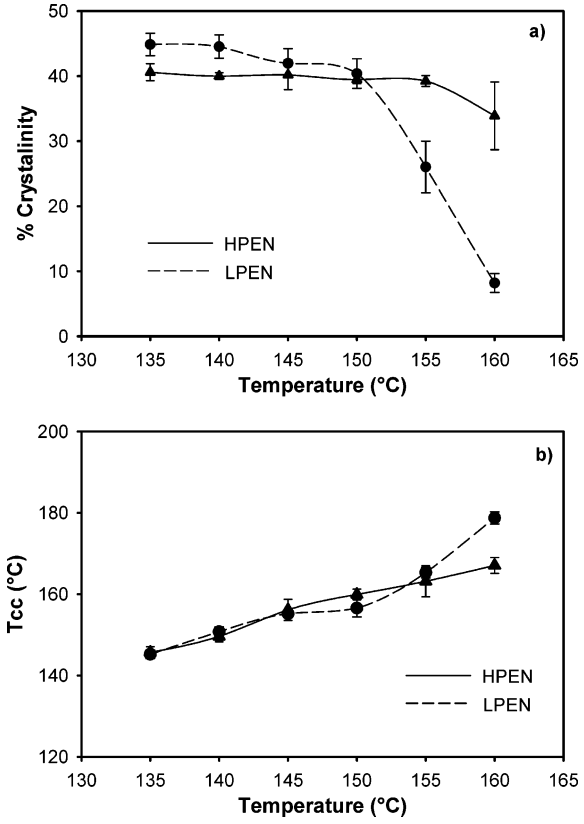

Figure 22. Temperature effect on the (a) percentage of crystallinity and (b) cold crystallization temperature. Results are presented for HPEN and LPEN stretched at 0.01 s^{-1} and total stretch ratio of 5×.

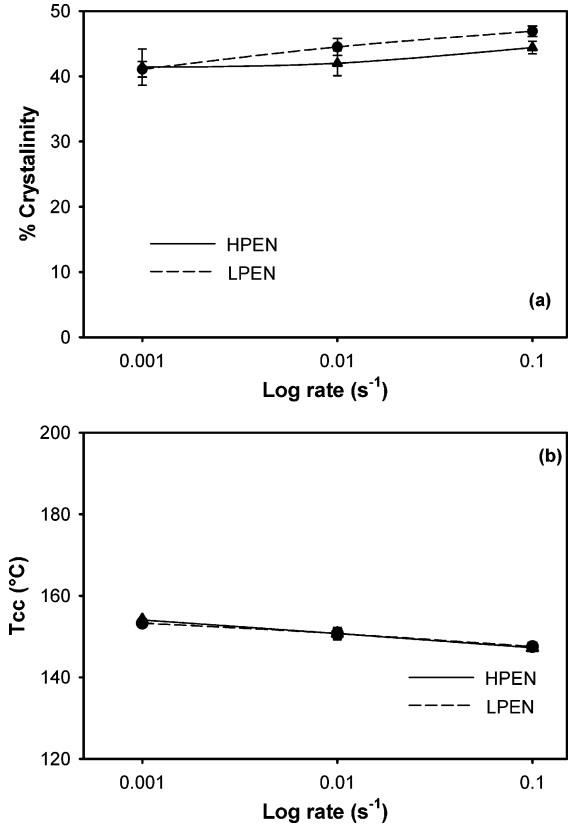

Figure 23. Rate effect on the (a) percentage of crystallinity and (b) cold crystallization temperature. Results are presented for HPEN and LPEN stretched at 140 °C and total stretch ratio of 5×.

weight. This directly translates to higher stress levels observed for HPEN as compared to LPEN under the same processing conditions.

Previously, the deviation from linearity of the stress optical rule was attributed to the crystallization of the material. At early stages of deformation of LPEN the T_{cc} cold crystallization peak splits into a bimodal peak (notice this at 1.7×). This suggests that early stages of stretching involves formation of two population of amorphous chains: one is the oriented population that crystallize at lower temperatures, and the other is the original relatively unoriented population that crystallize at higher temperatures. The unoriented population fraction rapidly diminishes with the increase of deformation as evidenced in the DSC curves. These results suggests that although the crystallinity is still relatively low (around 8%), the movement of T_{cc} toward T_g at low levels of deformation (below stretch ratios of 1.7×) indicates that the failure of the stress optical rule can be attributed to the orientation of amorphous population that establishes long range "telegraphic" connections with each other. The movement of T_{cc} with 1.7× is 13 °C for LPEN and 23 °C for HPEN, as shown in Figure 20. The splitting of T_{cc} is not present in HPEN, perhaps reflecting a more homogeneous distribution of stresses throughout the chains as it contains larger number of entanglements.

B. Effect of M_w, Temperature, and Rate. Figure 21 compares the WAXD patterns of the two molecular weight materials as a function of stretching conditions. Both materials were stretched for a series of temperatures and rates, as indicated in the figure to a total stretch ratio of 5×. The WAXS patterns surrounded with a bold rectangle corresponds to the samples for which the mechanical behavior was presented previously in Figures 5 and 6.

At intermediate stretching rate (0.01 s^{-1}), as the temperature increases, definition of off-equatorial planes improves indicating enhancement of translational order along the stretching direction (compare 130 vs 150 °C data). At about 160 °C for HPEN and 155 °C for LPEN the crystalline orientation decreases substantially.

These results are confirmed by DSC experiments, as shown in Figure 22. HPEN shows crystallinity around 40% at temperatures below 155 °C, whereas LPEN shows in average 45% crystallinity below 150 °C. A drop in crystallinity level is observed thereafter for both materials but with emphasis for LPEN that becomes lower that 10% at 160 °C. Accordingly, as the temperature increases, the T_{cc} of stretched samples moves toward T_{cc} of as-received material, respectively 190 °C for LPEN and 200 °C for HPEN. The efficiency of stress-induced crystallization is therefore reduced as temperature increase, as expected.

Comparison of X-ray patterns at high temperatures with the mechano-optical behavior of PEN shows that when the material behaves like taffy pull (Figure 5), it remains completely amorphous although it is stretched much more than at any other temperature. In addition, the stress and orientation levels are so low that it follows the stress−optical rule, i.e., the material remains in regime I of mechano-optical behavior (Figure 11b). At temperatures where the material substantially elongates and at last strain hardens, crystallization increases to approximately 20%, however, with very low crystalline orientation and stress optical behavior remaining in regime II.

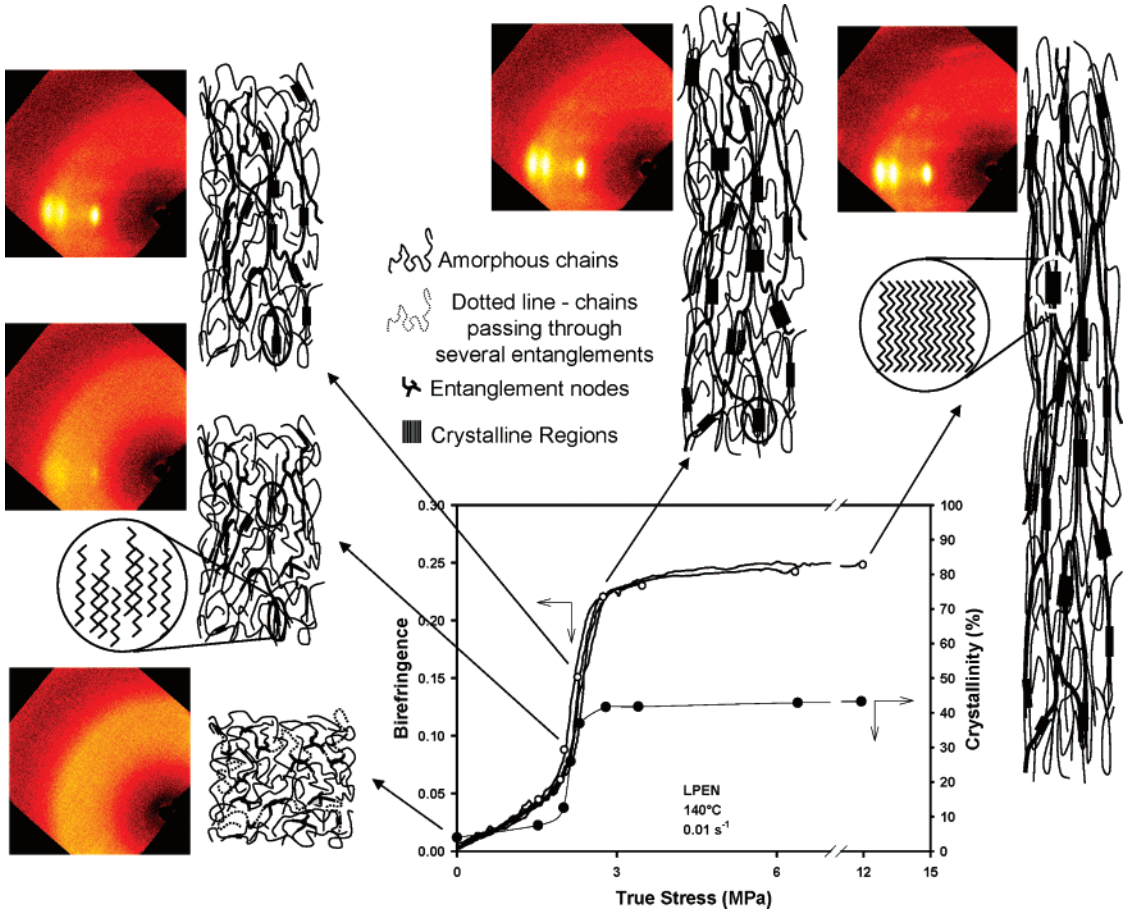

Figure 24. Structural model representative of PENs behavior under rubbery state deformation.

When analyzing the rate effect (Figure 21), it is possible to observe that no significant difference exists at temperatures below 145 °C for HPEN and 140 °C for LPEN. Both materials possess high level of crystallinity, as shown in Figure 23, ranging from 40% to 45% as the rate increases. Tcc reflects this result by a small decrease in its peak position when rate increases. The WAXD pattern, on the other hand, indicates that the molecules are highly oriented but with low crystalline perfection. As the rate increases the crystalline perfection slightly decreases.

At higher temperatures, the structure formation depends greatly on the rate. The orientation of the material decreases considerably with the decrease of rate, especially for LPEN.

The combination of high temperatures and low rates results in a completely amorphous structure for both molecular weight materials (see Figure 21 at 155 °C for HPEN and 150−155 °C for LPEN). Considering that the time needed for stretching the sample at 0.001 s^{-1} is approximately 70 min (including equilibration time) and that half-time crystallization of LPEN at 155 °C is approximately 30 min (see Figure 3), it means that thermal crystallization should have started during the stretching process; however, neither thermal crystallization nor stress inducing crystallization took place, resulting in a completely amorphous structure. At 160 °C, however, the WAXD pattern of LPEN shows the existence of crystalline ring, indicating the crystallization of the material in the absence of orientation. This shows that now thermal crystallization become significant.

Under the conditions where the material remains amorphous, the halftime of thermal crystallization is quite long and the orientation relaxation is sufficiently high, and this leads to unoriented amorphous structures even at the end of large deformation levels.

The difference in M_w becomes significant as the temperature increases (above 145 °C) or rate decreases (below 0.01 s^{-1}), as LPEN exhibit lower orientation as compared to HPEN as a result of lower entanglement density of LPEN that promotes substantial mechanisms of chain slippage and disentanglement. Therefore, these mechanisms will affect and delay the formation of a network and in turn manifest itself mechanically as taffy pull.

Structural Model. On the basis of the experimental observation mentioned above, a model depicting the structural hierarchy or structural mechanism evolution from the amorphous state to the final crystalline state is proposed. This model is illustrated in Figure 24.

At the initiation of deformation, the polymer chains are unoriented and amorphous, and they remain in the amorphous state throughout regime I where they obey the linear stress optical rule. Development of small fraction of domains wherein chains with extreme orientation exhibiting nematic-like order ends regime I and starts regime II. At this point the crystallinity level, as detected by the DSC, is less than 10%, and X-rays detect nematic-like ordered oriented by highly distorted crystallites. These small and highly distorted crystallites together with the entanglement nodes already existing in the amorphous structure will start the formation of a long-range network. Effectiveness of chain orientation

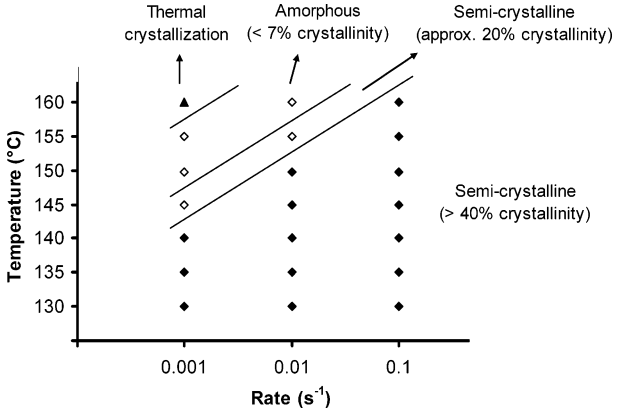

Figure 25. Dynamic phase diagram of PEN films as a function of temperature and rate.

improves substantially with the occurrence of this mechanism because the chains can be constrained between several nodes of the network, thereby increasing the efficiency of force transmission throughout the material leading to rapid birefringence increase. The molecules that are interconnected through these nodes will become extremely aligned, as seen by the WAXD pattern of LPEN. However, the poor translational alignment of the chains prevents them from fast crystallization. As deformation further proceeds, crystallization is promoted, which in turn tightens the network structure as an autocatalytic effect. This mechanism is illustrated in Figure 10 by the fast increase of birefringence in regime II, along with the appearance of very sharp crystalline reflections in the equatorial position and the increase of crystallinity to around 40%. Eventually, chains approach their extensibility limit, leading to leveling off of birefringence while stresses continue to rise. This point coincides with the strain hardening point of the material.

The temperature and rate effect play an important role on the structural development of PEN and final texture obtained. In the range of temperatures and rates studied most of the conditions used results in crystalline structure; however, amorphous structure can also be obtained at very special conditions, such as high temperatures and low rates where substantial relaxations are coupled with relatively slow thermal crystallization behavior. Figure 25 maps the dependency of temperature and rate on the structural formation of PEN films stretched in the rubbery state.

Conclusions

The influence of temperature, rate, and molecular weight on linear and nonlinear stress optical behavior of PEN deformed in the rubbery state was mapped. At low rates and deformation levels, regime I that is identified as the traditional stress optical rule regime is observed, and its slope is independent of molecular weight, rate, and temperature with the exception of temperatures very near the glass transition temperature. Stretching at intermediate stretch ratios and higher rates leads to transition to regime II which manifests itself as rapidly increasing birefringence coupled with moderate stress increases. The main cause of this regime is the spontaneous deformation due to coil-to-stretch transition manifesting as a fast deformation rate regime that also accompanies formation of strain-induced crystallites. When the chains reach their limit of extensibility, the birefringence levels off while stress continues to increase. The latter defines the last regime III where the little increase in birefringence and crystal chain orientation is observed. At these high deformation levels, a tight network structure is fully developed, suppressing the large changes in birefringence.

Stretching rate, temperature, and molecular weight were shown to have dramatic influence on the stress−optical properties and consequent structural development. If sufficiently low rates are used at high temperatures, no crystallization is observed and the material exhibits taffy-pull character. When stretched at high rates and lower temperatures, the structure tend to be composed of crystallites lacking three-dimensional order.

Acknowledgment. We thank FCT − the Portugese Science and Technology Foundation and FSE−III Framework Programme−European Commission for providing financial support to C. I. Martins during her PhD program at the University of Akron.

References and Notes

(1) Cakmak, M.; Lee, S. W. *Polymer* **1995**, *36*, 4039−4053.
(2) Cakmak, M.; Wang, Y. D.; Simhambhatla, M. *Polym. Eng. Sci.* **1990**, *30*, 721−733.
(3) Cakmak, M.; Kim, J. C. *J. Appl. Polym. Sci.* **1997**, *65*, 2059−2047.
(4) Bicakci, S.; Cakmak, M. *Polymer* **1998**, *39*, 5405−5420.
(5) Beers, A.; Cakmak, M.; Min, K. *ANTEC Conf. Proc.* **1999**, 1667−1671.
(6) Bedia, E.; Murakami, S.; Kitade, T.; Kohjiya, S. *Polymer* **2001**, *42*, 7299−7305.
(7) Yoshioka, T.; Tsuji, M.; Kawahara, Y.; Kohjiya, S. *Polymer* **2003**, *44*, 7997−8003.
(8) Ito, M.; Takahashi, M.; Kanamoto, T. *Polymer* **2002**, *43*, 3675−3681.
(9) Ito H.; Suzuki, K.; Kikutani, T. Nakayama, K. PPS 18 conference proceedings, Portugal, 2002.
(10) Murakami, S.; Nishikawa, Y.; Tsuji, M.; Kawaguchi, A.; Kohjiya, S.; Cakmak, M. *Polymer* **1995**, *36*, 291−297.
(11) Schoukens, G.; Verschuere, M. *Polymer* **1999**, *40*, 3753−3761.
(12) Blanton, T. N. *Powder Diffr.* **2002**, *17*, 125−131.
(13) Cakmak, M.; Kim, J. C. *J. Appl. Polym. Sci.* **1997**, *64*, 729−747.
(14) Miyata, K.; Kikutani, T.; Norimasa, O. *J. Appl. Polym. Sci.* **1997**, *65*, 1415−1427.
(15) Wu, G.; Li, Q.; Cuculo, J. A. *Polymer* **2000**, *41*, 8139−8150.
(16) Wu, G.; Liu, M.; Li, X.; Cuculo, J. A. *J. Polym. Sci., Part B: Polym. Phys.* **2000**, *38*, 1424−1435.
(17) Ulcer, Y.; Cakmak, M. *Polymer* **1997**, *38*, 2907−2923.
(18) Ulcer, Y.; Cakmak, M. *J. Appl. Polym. Sci.* **1996**, *62*, 1661−1678.
(19) Cakmak, M.; Robinette, I.; Schaible, S. J. *Appl. Polym. Sci.* **1998**, *70*, 89−108.
(20) Flory, P. J. *Proc. R. Soc. London*, *A* **1956**, *234*, 60.
(21) Keller, A. In *Crystallization of Polymers*; Dosier, M., Ed.; Kluwer: Dordrecht, p 1. *NATO Advanced Research Workshop*, Mons Belgium, 1992.
(22) Jakeways, R.; Klein, J. L.; Ward, I. M. I. *Polymer* **1996**, *37*, 3761−3762.
(23) Carr, P. L.; Timothy, M. N.; Ward, I. M. *Polym. Adv. Technol.* **1997**, *8*, 592−600.
(24) Gutiérrez, M. C. G.; Karger-Kocsis, J.; Riekel, C. *Macromolecules* **2002**, *35*, 7320−7325.
(25) Mahendrasingam, A.; Martin, C.; Fuller, W.; Blundel, D. J.; Oldman, R. J.; MacKerron, D. H.; Harvie, J. L.; Riekel, C. *Polymer* **2000**, *41*, 1217−1221.
(26) Ran, S.; Wang, Z.; Burger, C.; Chu, B.; Hsiao, B. S. *Macromolecules* **2002**, *35*, 10102−10107.
(27) Kawakami, D.; Hsiao, B. S.; Ran, S.; Burger, C.; Fu, B.; Sics, I.; Chu, B.; Kikutani, T. *Polymer* **2004**, *45*, 905−918.
(28) Blundel, D. J.; Mahendrasingam, A.; Martin, C. Fuller, W. *J. Mater. Sci.* **2000**, *35*, 5057−5063.
(29) Welsh, G. E.; Blundel, D. J.; Windle, A. H. *J. Mater. Sci.* **2000**, *35*, 5225−5240.

(30) Kawakami, D.; Hsiao, B. S.; Ran, S.; Burger, C.; Fu, B.; Sics, I.; Chu, B.; Kikutani, T. *Polymer* **2004**, *45*, 905−918.
(31) Koike, Y.; Cakmak, M. *Polymer* **2003**, *44*, 4249−4260.
(32) Valladares, D.; Toki, S.; Sen, T. Z.; Yalcin, B.; Cakmak, M. *Macromol. Symp.* **2002**, *185*, 149−166.
(33) Koike, Y.; Cakmak, M. *Macromolecules* **2004**, *37*, 2171−2181.
(34) Serhatkulu, T.; Cakmak, M. *ANTEC Conf. Proc.* **1999**, 1645−1649.
(35) Toki, S.; Valladares, D.; Sen, T. Z.; Cakmak, M. *ANTEC Conf. Proc.* **2001**, 1830−1834.
(36) Ouchi, I. H.; Aoki, S.; Shinotsuma, T.; Asai, M.; Hosoi, *Proc. 17th Japan Congr. Mater. Res*. March 1974, p 217.
(37) Mencik, Z. *Chem Prum.* **1967**, *17*, 78.
(38) Valladares, D.; Toki, S.; Sen, T. Z.; Yalcin, B.; Cakmak, M. *Macromol. Symp.* **2002**, *185*, 149−166.
(39) Koike, Y.; Cakmak, M. *Polymer* **2003**, *44*, 4249−4260.
(40) Cheng, S. Z. D.; Wunderlich, B. *Macromolecules* **1988**, *21*, 789−797.
(41) Buchner, S.; Wiswe, D.; Zachmann, H. G. *Polymer* **1989**, *30*, 480−488.
(42) Lee, S. W.; Cakmak, M. *J. Macromol. Sci., Phys.* **1998**, *B37*, 501−526.
(43) Hu, Y. S.; Rogunova, M.; Schiraldi, D. A.; Hiltner, A.; Baer, E. *J. Appl. Polym. Sci.* **2002**, *86*, 98−115.
(44) Mahendrasingam, A.; Martin, C.; Fuller, W.; Blundel, D. J.; Oldman, R. J.; Harvie, J. L.; MacKerron, D. H.; Riekel, C.; Engström, P. *Polymer* **1999**, *40*, 5553−5565.
(45) Inoue, T. *Kobunshi/High Polym.* **1999**, *48*, 4.
(46) Miyata, K.; Ito, H.; Kikutani, T.; Norimasa, O. *Sen-I Gakkaishi* **1999**, *55*, 542−551.
(47) Huijts, R. A.; Peters, S. M. *Polymer* **1994**, *35*, 3119−3121.
(48) Odell, J. A.; Keller, A.; Miles, M. J. *Polymer* **1985**, *26*, 1219−1226.
(49) Hunkeler, D.; Nguyen, T. Q.; Kausch, H. H. *Polymer* **1996**, *37*, 4257−4269.
(50) Ryu, D. S.; Inoue, T.; Osaki, K. *Polymer* **1998**, *39*, 2515−2520.
(51) Iizuka, N.; Yabuki, K. *Sen-I Gakkaishi* **1995**, *51*, 463−469.
(52) Inoue, T.; Matsui, H.; Murakami, S.; Kohjiya, S.; Osaki, K. *Polymer* **1997**, *38*, 1215−1220.
(53) Okamoto, M.; Kubo, H.; Kotaka, T. *Macromolecules* **1998**, *31*, 4223−4231.
(54) Buchner, S.; Wiswe, D.; Zachmann, H. G. *Polymer* **1989**, *30*, 480−488.

MA047499S